Geochemical Perspectives Letters

Diamond forms during low-pressure serpentinisation of oceanic lithosphere

N. Pujol-Solà, A. Garcia-Casco, J.A. Proenza, J.M. González-Jiménez, A. del Campo, V. Colás, A. Canals, A. Sánchez-Navas, J. Roqué-Rosell

Supplementary Information

The Supplementary Information includes:

- Geological Setting and Petrography
- Methods
- Tables S-1 and S-2
- Figures S-1 to S-7
- Supplementary Information References

Geological Setting and Petrography

The diamond-bearing samples were collected in the Potosí chromitite mining area (20°33'N, 74°45'W) within the Moa-Baracoa Ophiolitic Massif (MBOM; Fig. S-1a), eastern Cuba (Proenza *et al.*, 1999), which forms part of the ca. 1000 km long Cuban ophiolite belt (Late Jurassic - Cretaceous; Iturralde-Vinent *et al.*, 2016 and references therein). The MBOM consists of mantle harzburgites with subordinate dunites and a well-preserved Moho Transition Zone (MTZ), layered gabbros (Fig. S-1b) and mafic volcanic rocks (Marchesi *et al.*, 2006). The mantle tectonites of the MTZ contain elongate dunite bodies, chromitites and gabbroic sill intrusions following the fabric of the host harzburgite, as well as discordant dikes of gabbro, wehrlite and troctolite (Proenza *et al.*, 1999).

In the Potosí area, chromitite bodies are crosscut by several generations of gabbroic intrusions that locally triggered metasomatism in adjacent chromitites (Proenza *et al.*, 2001; González-Jiménez *et al.*, 2020; Pujol-Solà *et al.*, 2020). Diamond grains were found in a gabbro sill formed by a primary assemblage of

olivine (64% vol.; Fo_{74}), clinopyroxene (21% vol.; $En_{37-46}Wo_{49-41}Fs_{15-9}$), plagioclase (14% vol.; An_{59-64}), orthopyroxene (1% vol.; En_{74-75}) and accessory oxides that show a non-oriented coarse-grained magmatic texture (Figs. S-2, S-3, Table S-1). Diamond was also identified in interstitial magmatic olivine of associated chromitite bodies (Fig. S-4) described in detail by Pujol-Solà *et al.* (2020).

Methods

1. Sample preparation

Olivine gabbro and chromitite samples were collected from the Potosí area in the Moa-Baracoa massif, eastern Cuba. Thin sections were prepared at the University of Barcelona (UB) and the University of Granada (UGR). Thin sections were polished using diamond abrasive paste of 1 µm and 1/4 µm particle size and epoxy resin. Different sets of duplicated thin sections were prepared using Al_2O_3 or amorphous colloidal silica as carbon-free polishing materials in order to exclude contamination. In addition, ultrasonic baths were performed to remove any remaining polishing debris from the thin sections. Special doubly polished sections approximately 100 µm thick were also prepared for fluid inclusion studies using the same diamond abrasives and using polyester resin.

2. Scanning electron microscopy

Samples were studied in detail by optical microscopy and scanning electron microscopy, using a Quanta 200 FEI XTE 325/D8395 scanning electron microscope (SEM) and a JEOL JSM-7100 field-emission scanning SEM at the University of Barcelona (CCiTUB), and also using a GEMINI field-emission scanning SEM at the University of Granada. Operating conditions were 15 – 20 kV accelerating voltage and 5 nA beam current.

3. Electron probe microanalyses (EPMA)

Quantitative electron microprobe analyses (EMPA) were conducted at the CCiTUB using a JEOL JXA-8230 electron microprobe and in the Centre for Scientific Instrumentation of the University of Granada (CIC-UGR) using a CAMECA SX100 operated in wavelength-dispersive spectroscopy (WDS) mode. Analytical conditions were 20 kV accelerating voltage, 10-20 nA beam current, 1-2 µm beam diameter, and 10 s counting time per element. Natural and synthetic standards used were Cr_2O_3 (Cr), wollastonite (Si and Ca), corundum (Al), rutile (Ti), albite (Na), periclase (Mg), hematite (Fe), rhodonite (Mn), orthoclase (K), NiO (Ni), sphalerite (Zn), CaF (F), and NaCl (Cl) at the CCiTUB; and albite (Na), diopside (Si), wollastonite (Ca), vanadinite (Cl), sanidine (K), TiO_2 (Ti), rhodonite (Mn), CaF_2 (F), Fe_2O_3 (Fe), and synthetic periclase (Mg), Al_2O_3 (Al), Cr_2O_3 (Cr), and NiO (Ni) at the CIC-UGR. The correction procedure PAP (Pouchou and Pichoir, 1991) was used to convert specimen intensity ratios into concentrations. The chemical data for Cr-spinel were stoichiometrically recalculated in order to distinguish FeO from Fe_2O_3 according to the procedure described by Carmichael (1966).

X-ray maps of selected areas were collected with the CAMECA SX100 machine on thin sections using the following analytical conditions: 20 kV accelerating voltage, 300 nA beam current, focused spot, stage-scanning mode, 2 - 8 µm pixel size, and 20 - 30 ms counting time per pixel. The following elements were

mapped: Si, Al, Ba, Ti, Cr, Na, Mg, Mn, Fe, Ni, Ca, K, Cl, Zr, Zn, P, S, and O. The images were treated with DWImager software (Torres-Roldán and Garcia Casco, unpublished; see Garcia-Casco, 2007) and consist of the X-Ray signals of the elements (colour-coded; expressed in counts) and with polish defects, voids and all other mineral masked out. A grey-scale base-layer, calculated with the expression $\Sigma(counts_i \cdot A_i)$ (where A is atomic number, and i is Si, Ti, Al, Cr, Fe, Mn, Mg, Ca, Na and K), underlies the images and contains the basic textural information of the scanned areas. Phase abundance maps were created after the manipulation of the histograms of elemental maps.

4. Micro-Raman spectroscopy

Micro-Raman spectra of the solid and fluid inclusions in olivine were obtained using different instruments: a) HORIBA JobinYvon LabRam HR 800 dispersive spectrometer equipped with an Olympus BXFM optical microscope at CCiTUB. Non polarized Raman spectra were obtained in confocal geometry by applying a 532 nm laser, using a 100x objective (beam size around 2 µm), with 3 - 5 measurement repetitions for 10 - 15 seconds each. The Si band at ~520 cm^{-1} was used for calibration. The obtained spectra were processed using the LabSpec® software (JobinYvon; Villeneuve-d'Ascq, France); b) JASCO NRS-5100 dispersive spectrometer equipped with an Olympus Optical microscope at CIC-UGR. The spectra conditions were the same as above. The obtained spectra were processed using the Spectra Manager™ II Software and KnowItAll® JASCO Software. The micro-Raman maps were made in two-dimensional mode in the thin sections with 1 µm step and focus at different depth.

Mapping and cross-sections of selected inclusions were taken with a confocal Raman microscope (CRM) at the Instituto de Cerámica y Vidrio (CSIC – Madrid) with spectral resolution of 0.02 cm^{-1}, coupled with an AFM instrument (Witec ALPHA 300RA), with laser excitation at 532 nm and a 100× objective lens (NA = 0.95). The incident laser power was 2 - 6 mW. The optical diffraction resolution was limited to about 200 nm laterally and 500 nm vertically. The samples were mounted in a piezo-driven scan platform having 4 nm lateral and 0.5 nm vertical positioning accuracy, also equipped with an active vibration isolation system, active 0.7 - 1000 Hz. The images were processed and analysed with the software WiTec Project Plus 2.08.

Some inclusions below the polished mineral's surface do not show Raman signal of CH_4 (or of any other gas species) probably related to the low density of the gas within the inclusion and the detection limit of the Raman analyses (see Grozeva *et al.*, 2020).

5. Focused ion beam (FIB)

A selected inclusion containing diamond hosted in the olivine gabbro was prepared as an electro-transparent thin-foil at the Barcelona Research Center in Multiscale Science and Engineering, from the Polithecnical University of Catalonia (UPC), using a double-beam workstation (Neon40, CarlZeiss) equipped with a Schotky FE-SEM and FIB Ga^+ columns. The selected inclusion was coated with a thin slip (~100 nm) of Pt by means of e-beam assisted gas deposition as a protection layer for milling and polishing of the thin-foil. Then, the sample was milled by means of Ga ion bombardment until 1 µm thickness. The thin-foil was then lift-out and transferred to a TEM grid using a Kleindiek® micromanipulator with a tungsten tip and fixed into the TEM grid by ion-beam assisted Pt deposition. Finally, the inclusion area within the thin-foil was polished until electron transparency was achieved (down to ~80 µm).

A second diamond inclusion within olivine from chromitite was prepared as a thin-foil at the Laboratorio de Microscopías Avanzadas (LMA) from the Universidad de Zaragoza, using a dual beam

Helios Nanolab 650 equipped with a FE-SEM and FIB Ga^+ column. For the thin-foil preparation, the thin section was firstly coated with a thin (a few µm) layer of Pd and the area of the inclusion was also coated with a Pt layer by means of e-beam assisted gas deposition for protection of the interest area. The preparation of the thin-foil followed the same process as described above, but it was transferred to the grid using an Omniprobe® nanomanipulator.

6. Transmission electron microscopy (TEM)

The TEM study on the first thin-foil (olivine gabbro) was performed at the CCiTUB with a JEOL JEM-2100 LaB_6 transmission electron microscope (TEM) with energy dispersed analysis of X-rays (EDX), operated at 200 kV in STEM mode and beam size of ~15 nm, with an Oxford Instruments INCA x-sight spectrometer with Si (Li) detector. Images were acquired using a Gatan CCD Camera Orius SC1000 and processed with the DigitalMicrograph™ Software (v. 1.71.38).

The second thin-foil (chromitite) was studied using a FEI Titan G2 TEM equipped with Field Emission cannon XFEG, with spherical correction for the objective lens and working at 300 kV at the CIC-UGR. The microscope is equipped with four energy-dispersive analyses of X-rays (EDX) detectors (FEI microanalysis Super X) that allowed to perform elemental maps, and high angle-annular dark field detector (HAADF) that allowed to obtain high Z contrast mages. High-magnification electron microscopy (HMEM) images and selected area electron diffraction (SAED) patterns were also acquired. Images were processed with Digital Micrograph® Software (v. 1.71.38) and maps with INCA® Microanalysis Suite Software (v. 4.09).

7. Electron energy loss spectroscopy (EELS)

The electron energy loss spectroscopy (EELS) was performed at the CIC-UGR using a Zeiss Libra 120 plus LaB_6 transmission electron microscope with Omega energy filtering, operating at 120 kV. Analyses were done at 80000x magnification with 1 - 2 µA current emission on an area of 300 nm of diameter.

8. Thermodynamic calculations

The thermodynamic calculations were performed using Perple_X 6.8.3 (Connolly, 2009; http://www.perplex.ethz.ch/) and the internally consistent thermodynamic database of Holland and Powell (2011) extended to include super-reduced phases (cr_hp11ver_metal.dat). In the above database we removed graphite in order to simulate the metastable formation of diamond. The solution models considered were olivine (Holland and Powell, 1998) and C-O-H fluid (Connolly and Cesare, 1993). All other minerals involved in the calculations were treated as pure phases. Phase relations for olivine-hosted CH_4-rich fluid inclusions were computed at 100 MPa and 350 ºC in the system $MgO\text{-}FeO\text{-}SiO_2\text{-}C\text{-}O_2\text{-}H_2$ (MFSCOH). The bulk composition of the fluid inclusion-olivine ensemble corresponds to an initial assemblage of 0.7:0.3 molar mix of magmatic olivine (Fo_{74}, $(Mg_{1.48}Fe_{0.52})SiO_4$) and H_2O-rich fluid (X_{H2O} = 0.95, $0.95H_2O{:}0.05CO_2$). The phase relations for diamond-COH fluid (Fig. 3) were computed in the C-O-H system and contoured for oxygen fugacity isopleths calculated for a diamond-buffered fluid (Connolly and Cesare, 1993).

Tables S-1 to S-2

Table S-1 Representative electron microprobe analyses of olivine in the studied samples.

Sample	POT-2(II)					POT-2B					POT-3				
Analyse	**ol-1**	**ol-2**	**ol-3**	**ol-4**	**ol-5**	**ol-1**	**ol-2**	**ol-3**	**ol-4**	**ol-5**	**ol-1**	**ol-2**	**ol-3**	**ol-4**	**ol-5**
SiO_2 (wt.%)	38.26	38.17	38.03	37.70	37.75	37.59	37.55	37.45	37.65	38.02	40.54	40.47	40.68	40.49	40.59
TiO_2	bdl	bdl	bdl	bdl	bdl	0.02	bdl	bdl	0.02	bdl	bdl	bdl	bdl	bdl	0.02
Al_2O_3	bdl	bdl	bdl	bdl	bdl	bdl	0.02	0.03	bdl	bdl	bdl	bdl	0.02	bdl	0.03
Cr_2O_3	bdl	bdl	bdl	bdl	bdl	bdl	bdl	bdl	bdl	bdl	bdl	0.06	0.05	0.03	bdl
FeO_t	24.03	24.19	24.23	24.15	24.22	24.78	24.33	24.70	24.30	24.28	9.90	9.96	9.61	10.03	9.70
MnO	0.35	0.34	0.36	0.37	0.36	0.36	0.39	0.38	0.38	0.38	0.14	0.16	0.16	0.17	0.16
MgO	37.79	37.76	37.45	37.34	37.47	36.80	36.80	36.47	36.86	37.25	48.75	48.55	48.70	48.94	48.74
NiO	0.15	0.14	0.16	0.15	0.16	0.14	0.18	0.15	0.12	0.15	0.27	0.28	0.26	0.28	0.29
CaO	0.05	0.04	0.03	0.02	0.03	0.03	0.03	0.05	0.04	0.02	0.02	0.02	0.02	0.03	0.02
Total	100.63	100.64	100.26	99.73	99.99	99.73	99.31	99.23	99.37	100.10	99.62	99.49	99.50	99.97	99.55
Cations per 4 oxygens															
Si	0.997	0.996	0.996	0.994	0.993	0.994	0.995	0.995	0.997	0.998	0.999	0.998	1.002	0.995	0.999
Ti						0.000			0.000						0.000
Al							0.001	0.001					0.001		0.001
Cr												0.001	0.001	0.001	
Fe^{2+}	0.524	0.528	0.531	0.532	0.533	0.548	0.539	0.549	0.538	0.533	0.204	0.206	0.198	0.206	0.200
Mn	0.008	0.008	0.008	0.008	0.008	0.008	0.009	0.008	0.009	0.008	0.003	0.003	0.003	0.004	0.003
Mg	1.468	1.469	1.463	1.467	1.469	1.450	1.454	1.445	1.455	1.458	1.790	1.786	1.787	1.792	1.789
Ni	0.003	0.003	0.003	0.003	0.003	0.003	0.004	0.003	0.003	0.003	0.005	0.005	0.005	0.005	0.006
Ca	0.001	0.001	0.001	0.001	0.001	0.001	0.001	0.001	0.001	0.001	0.000	0.000	0.000	0.001	0.001
Total	3.002	3.004	3.003	3.006	3.007	3.005	3.003	3.003	3.002	3.001	3.001	3.000	2.997	3.003	2.999
Fo	0.74	0.74	0.73	0.73	0.73	0.73	0.73	0.72	0.73	0.73	0.90	0.90	0.90	0.90	0.90
Ni (ppm)	1288	1143	1366	1257	1310	1137	1529	1301	1040	1260	2309	2323	2178	2319	2468

Table S-2 Selected representative studied inclusions in olivine from the Potosí gabbro (POT-2) and chromitite (POT-3).

						Species												
Sample	Host rock	Number	In surface/ sealed	Inclusion abundance	Size (μm)	Lizardite	Polygonal serpentine	Magnetite	CH_4	cm^{-1}	H_2	cm^{-1}	Amorphous C / graphite	Diamond	cm^{-1}	Calcite	Clinopyroxene	Chlorite	Native Si
POT-2(II)	Gabbro	1	Surface	++	4			X						X	1332	X			
POT-2(II)	Gabbro	2	Surface	++	2			X						X	1328	X			
POT-2(II)	Gabbro	3	Surface	++	4			X					X	X	1328				
POT-2(II)	Gabbro	4	Surface	++	6			X						X	1326	X			
POT-2(II)	Gabbro	5	Surface	++	5			X					X	X	1330				
POT-2(II)	Gabbro	6	Surface	+++	1								X			X			
POT-2_Al	Gabbro	7	Sealed	++	4			X	X	2913									
POT-2_Al	Gabbro	8	Sealed	++	4			X											
POT-2_Al	Gabbro	9	Sealed	++	4				X	2915									
POT-2B_Si	Gabbro	10	Sealed	++	4	X		X											
POT-2B_Si	Gabbro	11	Sealed	++	4	X		X											
POT-2B_Si	Gabbro	12	Sealed	++	4	X		X											
POT-2B_Si	Gabbro	13	Sealed	++	2	X		X											
POT-2B_Si	Gabbro	14	Sealed	++	2	X		X											
POT-2B_Si	Gabbro	15	Sealed	++	2	X													
POT-2B_Si	Gabbro	16	Sealed	++	2	X		X											
POT-2B_Si	Gabbro	17	Sealed	++	2	X			X	2915									
POT-2B_Si	Gabbro	18	Sealed	++	2	X			X	2917									
POT-2B_Si	Gabbro	19	Surface	++	2	X													
POT-2B_Si	Gabbro	20	Sealed	++	3	X			X	2915									
POT-2B_Si	Gabbro	21	Sealed	++	3		X	X	X	2915									
POT-2B_Si	Gabbro	22	Sealed	++	2		X		X	2915									
POT-2B_Si	Gabbro	23	Sealed	++	2		X		X	2915									
POT-2B_Si	Gabbro	24	Sealed	++	2	X		X	X	2915									
POT-2B_Si	Gabbro	25	Sealed	++	1								X						
POT-2B_Si	Gabbro	26	Sealed	++	1	X		X	X	2913									
POT-2B_Si	Gabbro	27	Sealed	+	2	X			X	2915									
POT-2B_Si	Gabbro	28	Sealed	+	2		X		X	2915									
PO-2_IF	Gabbro	29	Sealed	+	2			X											
PO-2_IF	Gabbro	30	Sealed	++	5	X		X	X	2912			X	X	1330		X		
PO-2_IF	Gabbro	31	Surface	++	5				X				X	X					
PO-2_IF	Gabbro	32	Sealed	++	2	X			X	2913									
PO-2_IF	Gabbro	33	Sealed	++	2	X			X	2915									
PO-2_IF	Gabbro	34	Surface	++	2	X								X	1331				
PO-2_IF	Gabbro	35	Sealed	++	2									X	1330				
PO-2_IF	Gabbro	36	Sealed	+++	5			X	X	2919									
PO-2_IF	Gabbro	37	Sealed	+++	5			X											

						Species												
Sample	Host rock	Number	In surface/ sealed	Inclusion abundance	Size (μm)	Lizardite	Polygonal serpentine	Magnetite	CH_4	cm^{-1}	H_2	cm^{-1}	Amorphous C / graphite	Diamond	cm^{-1}	Calcite	Clinopyroxene	Chlorite	Native Si
PO-2_IF	Gabbro	38	Surface	+	5	X		X											
PO-2_IF	Gabbro	39	Surface	+	5	X													
PO-2_IF	Gabbro	40	Surface	++	2	X							X	X	1329				
PO-2_IF	Gabbro	41	Sealed	++	3	X		X	X	2915									
POT-2c	Gabbro	42	Surface	+	4			X											
POT-2c	Gabbro	43	Surface	+	2	X		X											
POT-2c	Gabbro	44	Sealed	++	5	X		X	X	2916									
POT-2c	Gabbro	45	Sealed	++	4	X		X	X	2916									
POT-2c	Gabbro	46	Sealed	++	4	X		X		2914									
POT-2c	Gabbro	47	Sealed	++	2	X			X	2916									
POT-2c	Gabbro	48	Sealed	++	4			X	X	2916									
POT-2c	Gabbro	49	Sealed	++	4	X		X	X	2916									
POT-2c	Gabbro	50	Sealed	++	5				X	2918									
POT-2c	Gabbro	51	Sealed	++	4				X	2919									
POT-2c	Gabbro	52	Sealed	++	4			X											
POT-2c	Gabbro	53	Sealed	++	4	X		X	X	2918									
POT-2c	Gabbro	54	Sealed	++	5				X	2919									
POT-2c	Gabbro	55	Sealed	++	4				X	2918									
POT-2c	Gabbro	56	Sealed	++	5			X	X	2918									
POT-2c	Gabbro	57	Sealed	++	5	X		X	X	2916									
POT-2c	Gabbro	58	Sealed	++	5	X		X	X	2916									
POT-2c	Gabbro	59	Sealed	+	1			X											
POT-2c	Gabbro	60	Sealed	+	3			X											
POT-2c	Gabbro	61	Sealed	++				X											
POT-2c	Gabbro	62	Sealed	++		X		X											
POT-2c	Gabbro	63	Sealed	++				X											
POT-2c	Gabbro	64	Sealed	++				X											
POT-2c	Gabbro	65	Sealed	++				X											
POT-2c	Gabbro	66	Sealed	++				X											
POT-2c	Gabbro	67	Sealed	++				X											
POT-2c	Gabbro	68	Sealed	++				X											
POT-2c	Gabbro	69	Sealed	++														X	
POT-2c	Gabbro	70	Sealed	++				X											
POT-2c	Gabbro	71	Sealed	++		X		X	X	2917									
POT-2c	Gabbro	72	Sealed	++		X		X	X	2917									
POT-2c	Gabbro	73	Sealed	++		X		X											
POT-2c	Gabbro	74	Sealed	++		X		X											
POT-2c	Gabbro	75	Sealed	++					X	2917									
POT-2c	Gabbro	76	Sealed	++		X		X											
POT-2c	Gabbro	77	Sealed	++		X		X	X	2917									
POT-2c	Gabbro	78	Sealed	++		X		X											
POT-2c	Gabbro	79	Sealed	++		X		X											

						Species												
Sample	**Host rock**	**Number**	**In surface/ sealed**	**Inclusion abundance**	**Size (μm)**	**Lizardite**	**Polygonal serpentine**	**Magnetite**	**CH_4**	**cm^{-1}**	**H_2**	**cm^{-1}**	**Amorphous C / graphite**	**Diamond**	**cm^{-1}**	**Calcite**	**Clinopyroxene**	**Chlorite**	**Native Si**
POT-2c	Gabbro	80	Sealed	++		X		X											
POT-2c	Gabbro	81	Sealed	++	4	X		X	X	2917									
POT-2c	Gabbro	82	Sealed	++		X		X											
POT-2c	Gabbro	83	Sealed	++		X		X											
POT-2c	Gabbro	84	Sealed	++		X		X											
POT-2c	Gabbro	85	Sealed	++		X		X											
POT-2c	Gabbro	86	Sealed	++				X											
POT-2c	Gabbro	87	Sealed	++		X		X											
POT-2c	Gabbro	88	Sealed	++		X		X											
POT-2c	Gabbro	89	Sealed	++		X		X											
POT-2c	Gabbro	90	Sealed	++	12	X			X	2917							X		
POT-2c	Gabbro	91	Sealed	++	6	X													
POT-2c	Gabbro	92	Sealed	++	7	X		X											
POT-3	Chromitite	93	Surface	+++	4									X	1331				X
POT-3	Chromitite	94	Sealed	+++	2	X		X											
POT-3	Chromitite	95	Sealed	+++	3									X	1329				
POT-3	Chromitite	96	Sealed	+++	5	X													
POT-3	Chromitite	97	Sealed	+++	3									X	1330				
POT-3	Chromitite	98	Sealed	+++	6									X					
POT-3	Chromitite	99	Sealed	+++	4						X	4154							
POT-3	Chromitite	100	Surface	+++	1														

Figures S-1 to S-7

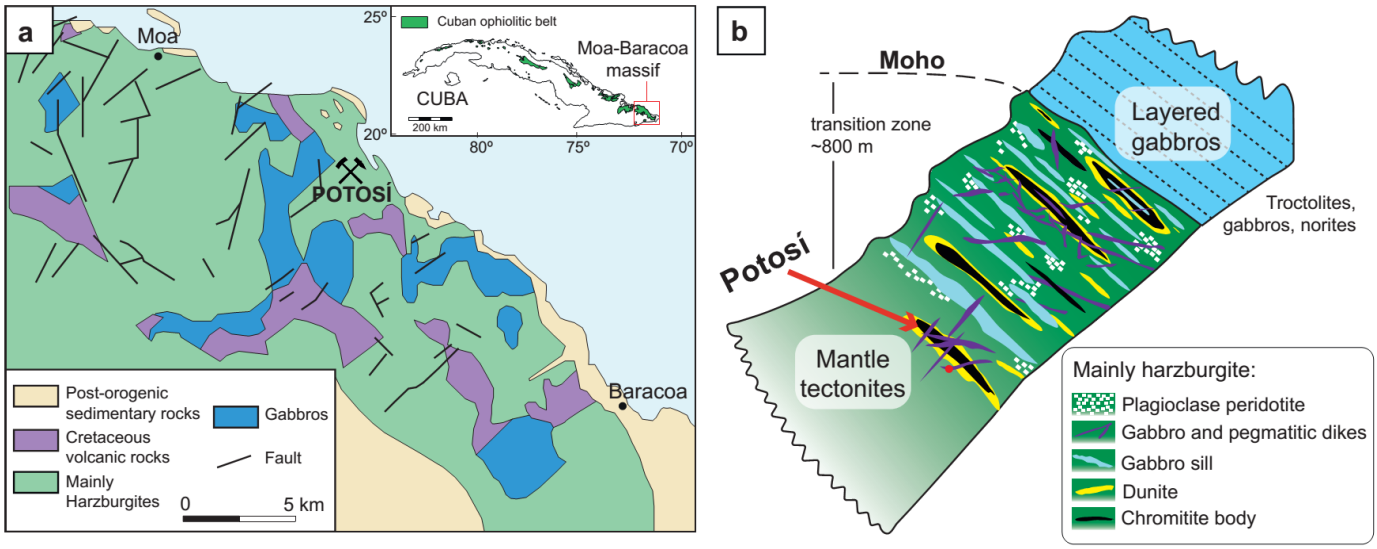

Figure S-1 **(a)** Geological map of the Moa-Baracoa massif in eastern Cuba, modified from Proenza *et al.* (2001). The inset in the upper right shows the location within the Cuba Island. **(b)** Schematic column of the ophiolitic sequence in the Moa Baracoa Massif (eastern Cuba) showing the position of the Potosí chromitites, modified from Marchesi *et al.* (2006).

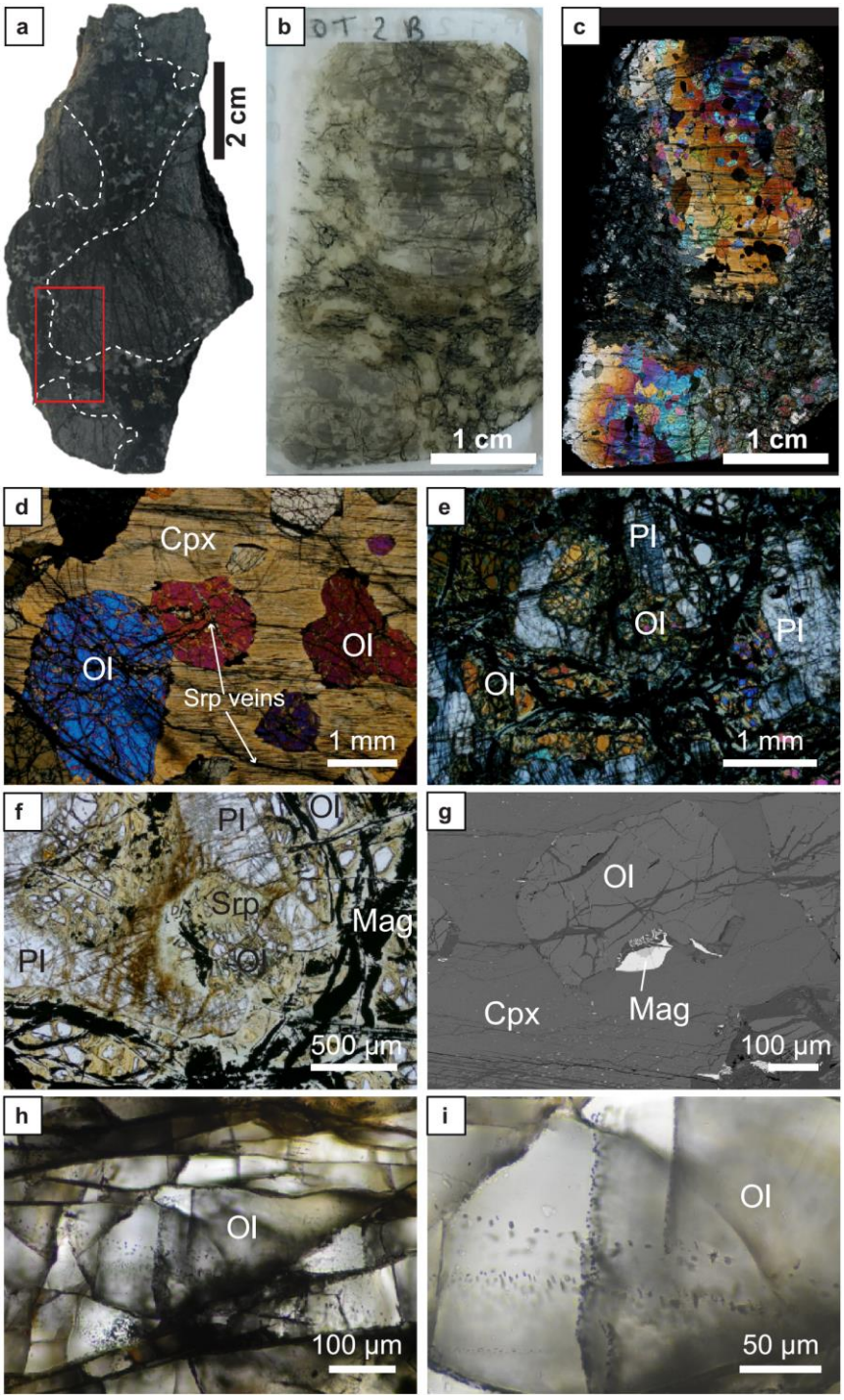

Figure S-2 **(a)** Diamond-bearing olivine gabbro hand sample. The red rectangle marks the area of the thin section in b-c. **(b)** Thin section of the olivine gabbro. **(c)** Thin section of the olivine gabbro in crossed nicols. Note the poikilitic texture of the sample. **(d)** Transmitted light (crossed nicols) photomicrograph of the olivine gabbro showing the poikikitic texture of clinopyroxene and olivine. **(e)** Transmitted light (crossed nicols) photomicrograph of the olivine gabbro showing the poikikitic texture of partially altered plagioclase and olivine. **(f)** Transmitted light photomicrograph of partially serpentinised olivine with serpentine-group minerals and magnetite veins. **(g)** Backscattered electron image of an olivine chadacryst with magnetite in a larger poikilitic clinopyroxene crystal. **(h)** Transmitted light photomicrograph of olivine hosting multiple trails of fluid inclusions with crosscutting relations. **(i)** Transmitted light photomicrograph of a close up of fluid inclusion trails hosted in olivine. Abbreviations: Cpx – clinopyroxene, Mag – magnetite, Ol – olivine, Pl – plagioclase, Srp – serpentine.

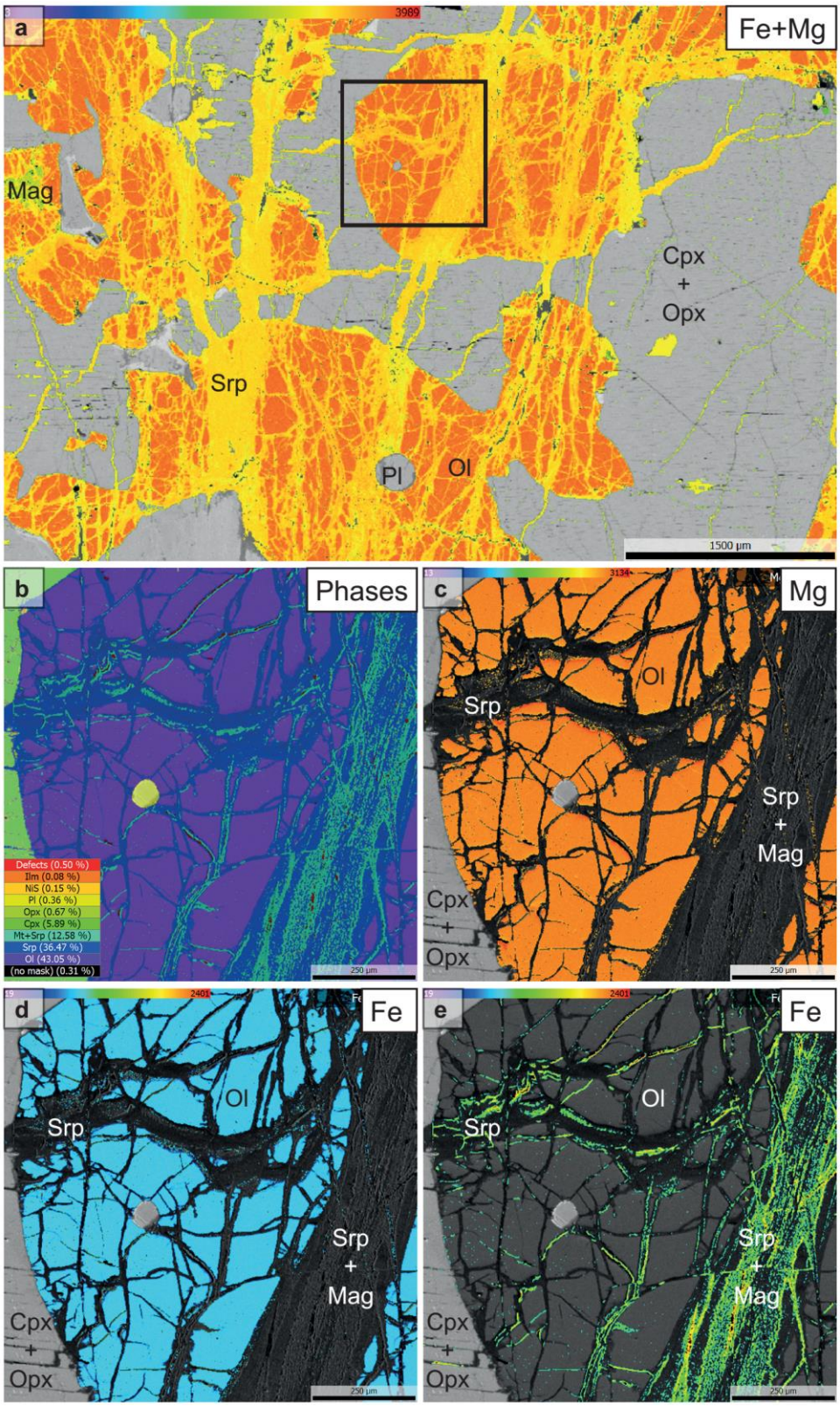

Figure S-3 Electron microprobe X-ray maps of the olivine gabbro. **(a)** Fe+Mg element map of olivine crystals and serpentine veins cross cutting the sample. The black square marks the area of the detailed maps b-e. **(b)** Phase map of the analysed area. **(c)** Mg map of olivine. **(d)** Fe map of olivine. **(e)** Fe map of the serpentine veins containing magnetite. Abbreviations: Cpx – clinopyroxene, Opx – orthopyroxene, Mag – magnetite, Ol – olivine, Pl – plagioclase, Srp – serpentine.

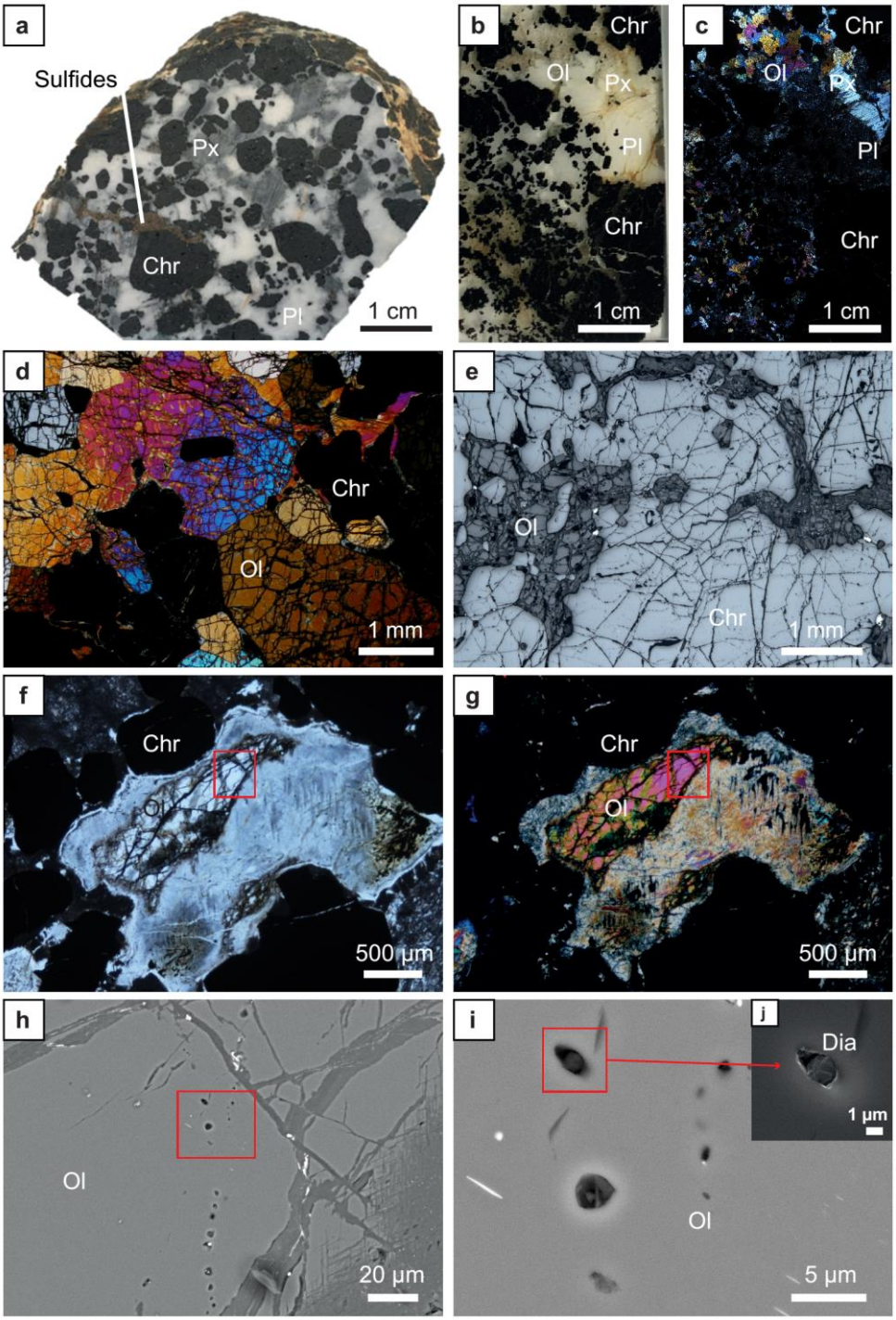

Figure S-4 **(a)** Diamond-bearing chromitite hand sample. **(b)** Thin section of the chromitite. **(c)** Thin section of the chromitite in crossed nicols. **(d)** Transmitted light (crossed nicols) microphotograph of chromitite showing intertitial magmatic olivine. **(e)** Reflected light microphotograph of chromite and interstitial olivine. **(f)** Transmitted light microphotograph of partially altered olivine hosting inclusion trails. **(g)** Transmitted light (crossed nicols) microphotograph of partially altered olivine hosting inclusion trails. The red rectangle marks the area of image h. **(h)** Backscattered electron image of inclusion trails hosted within olivine. The red rectangle marks the area of image i. **(i)** Backscattered electron image of inclusions hosting diamond and native Si (top) and serpentine (center): needle-like crystal is ilmenite and the bright dot is chromite. **(j)** Zoom of i showing a secondary electron image of the inclusion hosting diamond and native Si. Abbreviations: Chr – chromite, Dia - diamond, Mag – magnetite, Ol – olivine, Pl – plagioclase, Px – pyroxene.

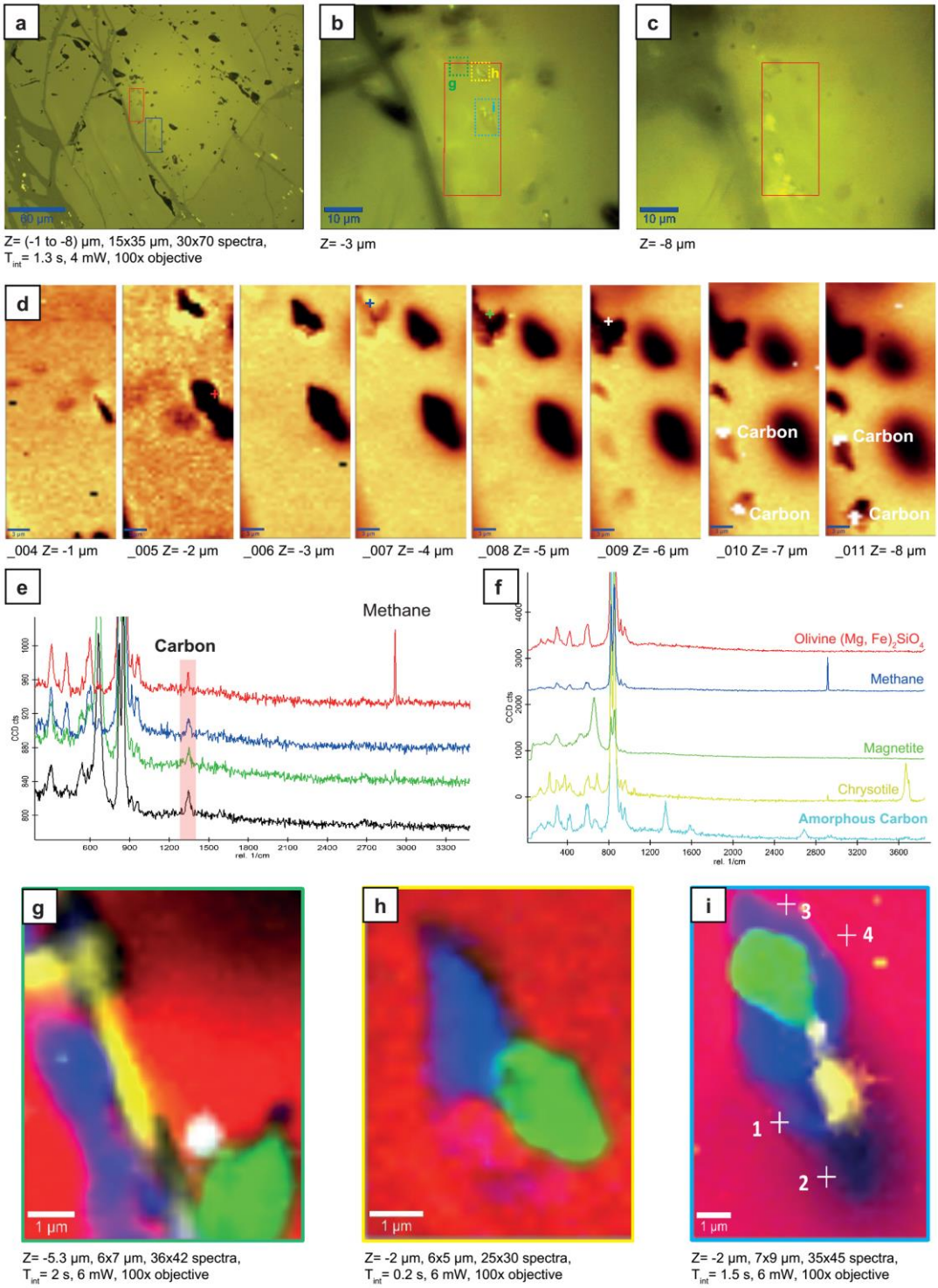

Figure S-5 Confocal Raman maps of fluid inclusions. **(a)** Reflected light microphotograph of inclusion trails hosted in olivine from the gabbro. **(b)** Zoom of a showing the inclusions at Z (depth) = -3 µm. **(c)** Image b with focus at Z = -8 µm. Note that the inclusions that are shown in b and c are different. **(d)** Z-stack in the area in red in b and c from Z = -1 µm to Z= -8 µm. Amorphous carbon has been recognized in 5 inclusions. **(e)** Amorphous carbon Raman patterns corresponding to the inclusions in the Z-stack of d. The colors correspond to the analyzed points showed in d. **(f)** Raman spectra for the different phases observed in the inclusion maps g-i. **(g)** X-Y Raman map of the inclusion denoted by the green square in b. **(h)** X-Y Raman map of the inclusion denoted by the yellow square in b. **(i)** X-Y Raman map of the inclusion denoted by the blue square in b.

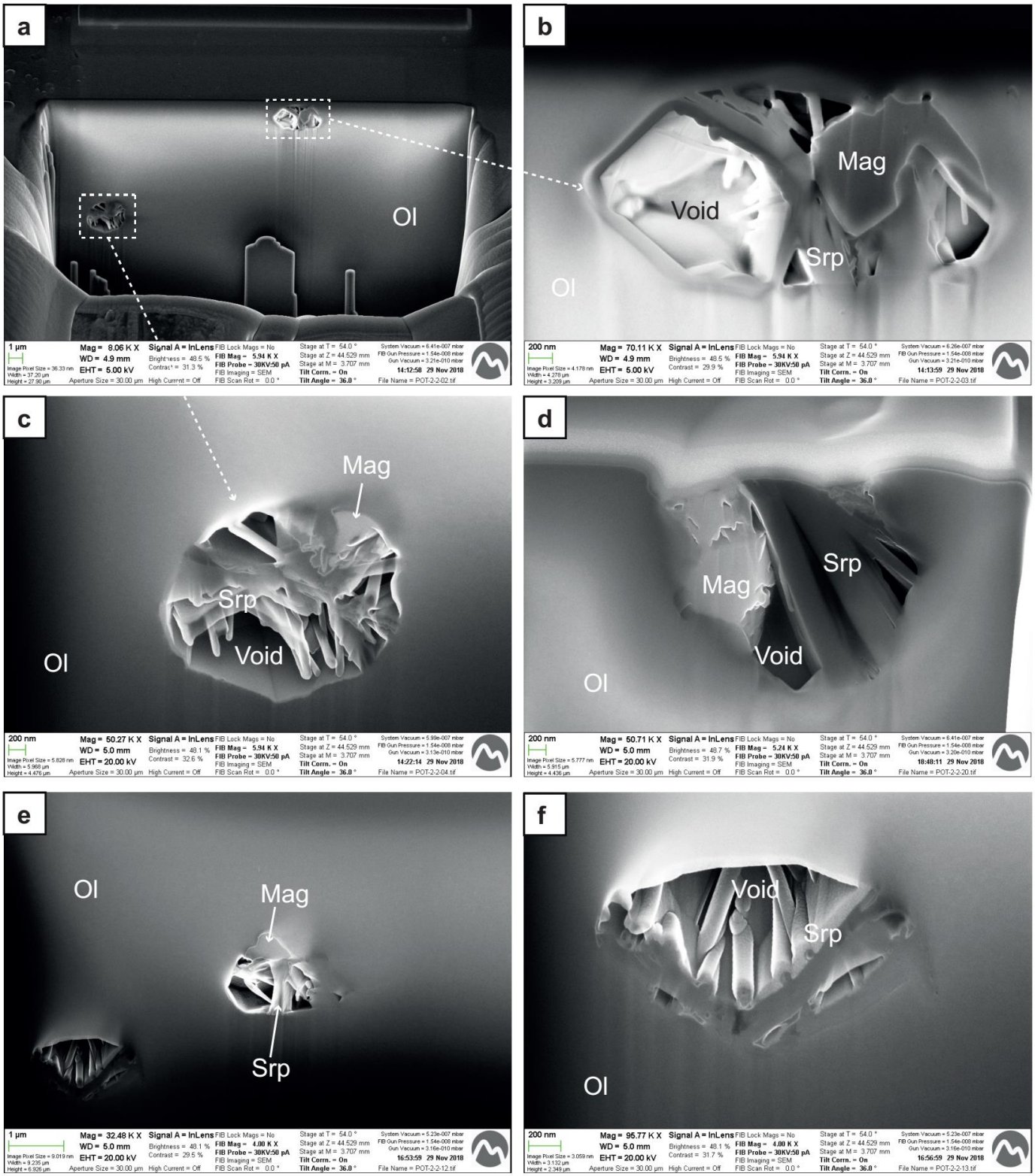

Figure S-6 Backscattered electron images of inclusions hosted within olivine cut with focused ion beam (FIB). Most inclusions contain serpentine and magnetite. Abbreviations: Mag – magnetite, Ol – olivine, Srp – serpentine.

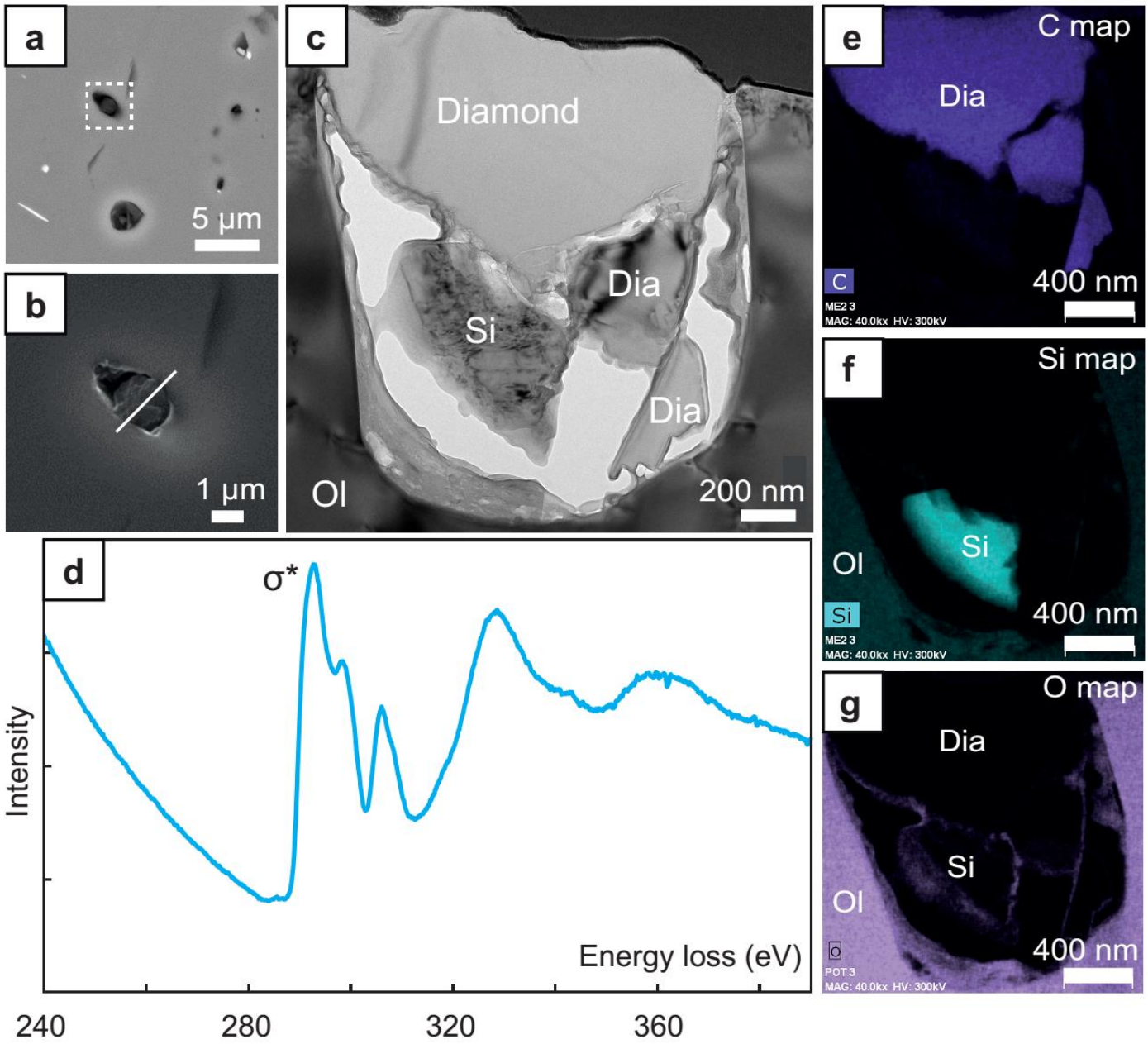

Figure S-7 Diamond hosted in interstitial olivine in chromitite. **(a)** Field-emission scanning electron microscope (FE-SEM) back-scattered image showing the location of a diamond grain in olivine. **(b)** Detailed FE-SEM secondary electron image of the diamond grain cut with focused ion beam (FIB). **(c)** Transmission electron microscopy (TEM) image showing the grains of diamond and native Si. **(d)** ELNES of C-K at the diamond grain, indicating the sp^3 hybridization of C by the presence of a strong σ* peak at about 290 eV, but no Π* peak. (**e-g**) TEM X-ray maps of C, Si and O, respectively. Abbreviations: Dia- diamond, Ol – olivine, Si – native silicon.

Supplementary Information References

Carmichael, I.S.E. (1966) The iron-titanium oxides of salic volcanic rocks and their associated ferromagnesian silicates. *Contributions to Mineralogy and Petrology* 14, 36–64.

Connolly, J.A.D. (2009) The geodynamic equation of state: What and how. *Geochemistry, Geophysics, Geosystems* 10.

Connolly, J.A.D., Cesare, B. (1993) C-O-H-S fluid composition and oxygen fugacity in graphitic metapelites. *Journal of Metamorphic Geology* 11, 379–388.

Garcia-Casco, A. (2007) Magmatic paragonite in trondhjemites from the Sierra del Convento mélange, Cuba. *American Mineralogist* 92, 1232–1237.

González-Jiménez, J.M., Proenza, J.A., Pastor-Oliete, M., Saunders, E., Aiglsperger, T., Pujol-Solà, N., Melgarejo, J.C., Gervilla, F., Garcia-Casco, A. (2020) Precious metals in magmatic Fe-Ni-Cu sulfides from the Potosí chromitite deposit, eastern Cuba. *Ore Geology Reviews* 118, 103339.

Grozeva, N.G., Klein, F., Seewald, J.S., Sylva, S.P. (2020) Chemical and isotopic analyses of hydrocarbon-bearing fluid inclusions in olivine-rich rocks. *Philosophical transactions. Series A, Mathematical, physical, and engineering sciences* 378, 20180431.

Holland, T.J.B., Powell, R. (1998). An internally consistent thermodynamic data set for phases of petrological interest. *Journal of Metamorphic Geology* 16, 309-343.

Holland, T.J.B., Powell, R. (2011) An improved and extended internally consistent thermodynamic dataset for phases of petrological interest, involving a new equation of state for solids. *Journal of Metamorphic Geology* 29, 333–383.

Iturralde-Vinent, M.A., Garcia-Casco, A., Rojas-Agramonte, Y., Proenza, J.A., Murphy, J.B., Stern, R.J. (2016) The geology of Cuba: A brief overview and synthesis. *GSA Today* 4–10.

Marchesi, C., Garrido, C.J., Godard, M., Proenza, J.A., Gervilla, F., Blanco-Moreno, J. (2006) Petrogenesis of highly depleted peridotites and gabbroic rocks from the Mayarí-Baracoa Ophiolitic Belt (eastern Cuba). *Contributions to Mineralogy and Petrology* 151, 717–736.

Pouchou, J.-L., Pichoir, F. (1991) Quantitative Analysis of Homogeneous or Stratified Microvolumes Applying the Model “PAP.” *Electron Probe Quantitation* 31–75.

Proenza, J., Gervilla, F., Melgarejo, J., Vera, O., Alfonso, P., Fallick, A. (2001) Genesis of sulfide-rich chromite ores by the interaction between chromitite and pegmatitic olivine -norite dikes in the Potosí Mine (Moa-Baracoa ophiolitic massif, Eastern Cuba). *Mineralium Deposita* 36, 658–669.

Proenza, J., Gervilla, F., Melgarejo, J.C., Bodinier, J.L. (1999) Al- and Cr-rich chromitites from the Mayari-Baracoa ophiolitic belt (Eastern Cuba): Consequence of interaction between volatile-rich melts and peridotites in suprasubduction mantle. *Economic Geology* 94, 547–566.

Pujol-Solà, N., Proenza, J.A., Garcia-Casco, A., González-Jiménez, J.M., Román-Alpiste, M.J., Garrido, C.J., Melgarejo, J.C., Gervilla, F., Llovet, X. (2020) Fe-Ti-Zr metasomatism in the oceanic mantle due to extreme differentiation of tholeiitic melts (Moa-Baracoa ophiolite, Cuba). *Lithos* 358–359, 105420.